PERGAMON

Journal of Structural Geology 24 (2002) 145–153

JOURNAL OF STRUCTURAL GEOLOGY

www.elsevier.com/locate/jstrugeo

Effects of local stress perturbation on secondary fault development

Laurent Maerten[a,*], Paul Gillespie[b], David D. Pollard[a]

[a]*The Rock Fracture Project, Stanford University, Stanford, CA 94305-2115, USA*
[b]*Norsk Hydro Research Center, Postboks 7190, N-5020 Bergen, Sweden*

Received 25 February 2000; revised 12 March 2001; accepted 20 March 2001

Abstract

The complex patterns of normal faults in sedimentary basins are commonly attributed to a complex geological history with varying directions of tectonic extension. However, we show an example of normal faulting from a North Sea hydrocarbon reservoir where the variability in secondary fault orientations can be attributed to stress perturbations that developed around the larger faults during a single phase of extension. This is demonstrated by comparing attributes of the stress fields computed around largest faults from detailed three-dimensional (3D) geomechanical models, with fault data such as discretized fault orientation and density observed from a high quality 3D seismic reflection survey. The modeling results show the strong influence of the irregular geometry (bends and intersections) of larger faults on the development of smaller faults. Methods developed in this study can be applied to predict likely locations and orientations of subseismic faults.

Keywords: North Sea tectonics; Normal faults; Subseismic faults; 3D numerical model; Extension; Stress field

1. Introduction

Highly variable fault strike direction or multiple fault sets in a given region are commonly observed at regional scale. Variability is often explained in terms of either multiple tectonic episodes, reactivation of pre-existing faults, or simultaneous development of faults under three-dimensional (3D) strain (Reches, 1983). Depending upon which explanation is chosen, geologists use observations of multiple fault sets to infer paleo-rotation of the regional stress field (Færseth et al., 1997), the trend of deeper faults, or the 3D strain field that caused faulting (Krantz, 1989).

Early studies, using analytical models (Hafner, 1951; Couples, 1977; Pollard and Segall, 1987), predict that a heterogeneous stress field can be caused by faulting. However, although the mechanical interaction of growing faults has been studied over the last 10 years (Willemse et al., 1996; Cowie, 1998; Gupta et al., 1998), the development of secondary faults in the vicinity of a larger fault has been the subject of few studies. Ackermann and Schlische (1997) ascribed the anticlustering of small normal faults to the stress-reduction shadow around larger faults observed in a quarry in the Mesozoic Danville basin in North Carolina. Sassi and Faure (1997) highlighted, through numerical experiments, the role played by major structural discontinuities in the local variations of stress regime and discussed the deformation modes of faulting and fracturing, which may take place at small scale.

In this paper we describe the spatial distribution (orientation and density) of faults from the Oseberg oil field area in the northern North Sea. Here, smaller normal faults, interpreted from seismic reflection surveys, strike in a wide variety of angles near larger faults. We hypothesize that the development of the smaller faults is related to the stress perturbation produced by displacement on the larger faults. We use 3D numerical models to predict the likely nucleation points and orientations of secondary faults, and show that stress perturbations can be observed at scales as large as the Viking Graben and not just at the small scale of an outcrop (Schlische et al., 1996; Ackermann and Schlische, 1997). Furthermore, the results illustrate how this concept can be used for the prediction of sub-seismic faults in aquifers or hydrocarbon reservoirs.

2. Geological setting

The Oseberg Syd reservoir is located in the Norwegian sector of the North Sea. This field, operated by Norsk Hydro, is located within Block 30/9 on the Norwegian Continental Shelf and forms part of the eastern flank of

* Corresponding author. Correspondence address (and now at): The Institut Français du Pétrole, 92852 Rueil-Malmaison Cedex, France. Tel.: +33-1-4752-6369; fax: +33-1-4752-7067.
E-mail address: laurent.maerten@ifp.fr (L. Maerten).

0191-8141/02/$ - see front matter
PII: S0191-8141(01)00054-2

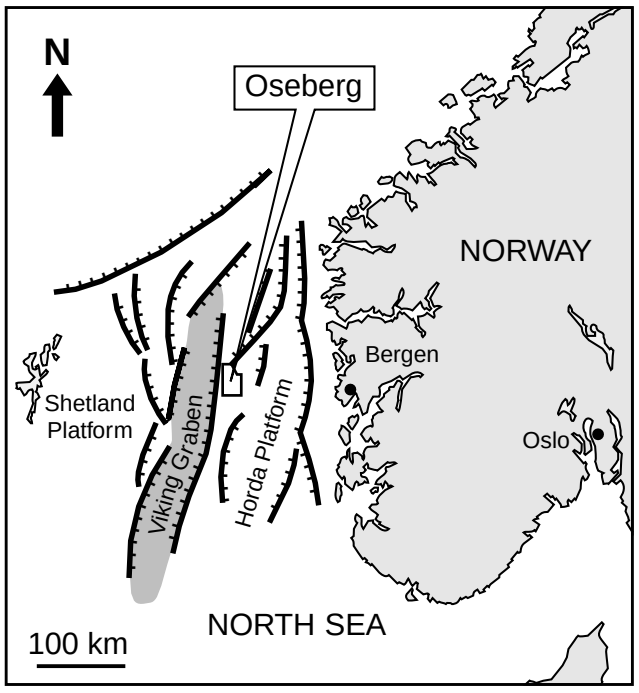

Fig. 1. Regional map showing the location of Oseberg Syd reservoir on the Norwegian Continental Shelf, northern North Sea. The study area forms part of the eastern flank of the Northern Viking Graben.

the Northern Viking Graben (Fig. 1). The structure has been well defined by 3D seismic reflection surveys. In essence, the area consists of a N–S to NNW–SSE striking, easterly tilted fault-block (the Oseberg fault-block) between the Horda Platform and the Viking Graben.

The Oseberg fault-block (Fig. 2) is defined by major west-dipping, N–S striking normal faults and southwest-dipping, NW–SE striking normal faults (Færseth and Ravnås, 1998). Fristad et al. (1997) have shown unequivocally that the larger faults in Oseberg Syd were active during sedimentation in Lower to Middle Jurassic times, with up to 100% thickness changes in the Brent, Dunlin and Statfjord Formations (see Fig. 2b and also see Fig. 4 in Fristad et al., 1997). Although the majority of the extension occurred in the Upper Jurassic (Kimmeridgian–Volgian), earlier extension is well documented in the North Sea (Yielding et al., 1992). The faults are typically truncated by an unconformity at the base of the Cretaceous, that dips to the west (see Fig. 2b).

Most of the largest faults in the study area (maximum displacements >250 m, gray in Fig. 2a) are ~N–S striking as shown on the rose diagram of Fig. 2c. On the basis of sedimentary thickness variations, we conclude that these faults were active from Lower to Upper Jurassic. Smaller faults (250 m > maximum displacements > 30 m, black in Fig. 2a) with much more variable orientation developed later, predominantly in the Upper Jurassic (Fristad et al., 1997), while the major faults were still active. Examination of Fig. 2a shows that orientations of the smaller faults with respect to the larger faults is not consistent across major fault blocks, suggesting that the orientations of the smaller faults were controlled by stress perturbations around the larger faults rather than by the stress conditions of successive tectonic events. Fig. 2d shows that smaller fault orientation is highly variable, ranging from N115° to N35°.

In the following numerical analysis, we aim to test the hypothesis that the later, smaller faults were influenced by the perturbed stress field around the earlier, larger faults by comparing attributes of the computed perturbed stress field around the larger faults to the strike and density of the smaller faults.

3. Numerical analysis

In geomechanical studies, one of the simplest idealizations of faulted rock is to approximate the rock mass of the upper crust as a homogeneous isotropic linear-elastic material cut by discontinuities that accurately represent the geometry of the seismically mapped faults. This approximation ignores the sedimentological heterogeneities and focuses attention on the structural heterogeneities (the seismically resolvable faults), their complex geometry and displacement. Our models, which capture the mechanics of an idealized single slip event or a series of events that do not include any stress relaxation, suggest likely locations where inelastic strains may accumulate, but do not characterize the inelastic deformation itself. Our underlying assumption is that these approximations capture the first-order relationship among fault geometry, fault displacement distributions, and perturbed stress field. The efficiency of this approach and its assumptions have been demonstrated through examples described by Willemse (1997), Maerten et al. (1999), Crider and Pollard (1998), Kattenhorn et al. (2000), Maerten et al. (2000), and Maerten (2000).

We have carried out geomechanical elastic modeling using the computer program Poly3D (Thomas, 1993), a 3D boundary element program based on the displacement discontinuity method and the governing equations of linear elasticity theory (Crouch and Starfield 1983; Becker, 1992). The 'boundary' surfaces are discretized as polygonal elements that are particularly well-suited to model complex surfaces such as a curving fault with irregular tip-line (Fig. 3).

The boundary conditions of a Poly3D model are of two types. The first corresponds to a constant displacement discontinuity, which is specified for each polygonal element of the fault surface. It can be decomposed into three components. The component normal to an element plane may represent the local opening along a joint, whilst the two components parallel to the element plane may represent the local dip-slip or strike-slip along a fault. By joining many small elements together, smooth displacement distributions can be approximated over each fault surface. The second type of boundary condition is a remote loading that can be strain or stress (Fig. 3). Usually, regional tectonic history of the modeled area, which may indicate

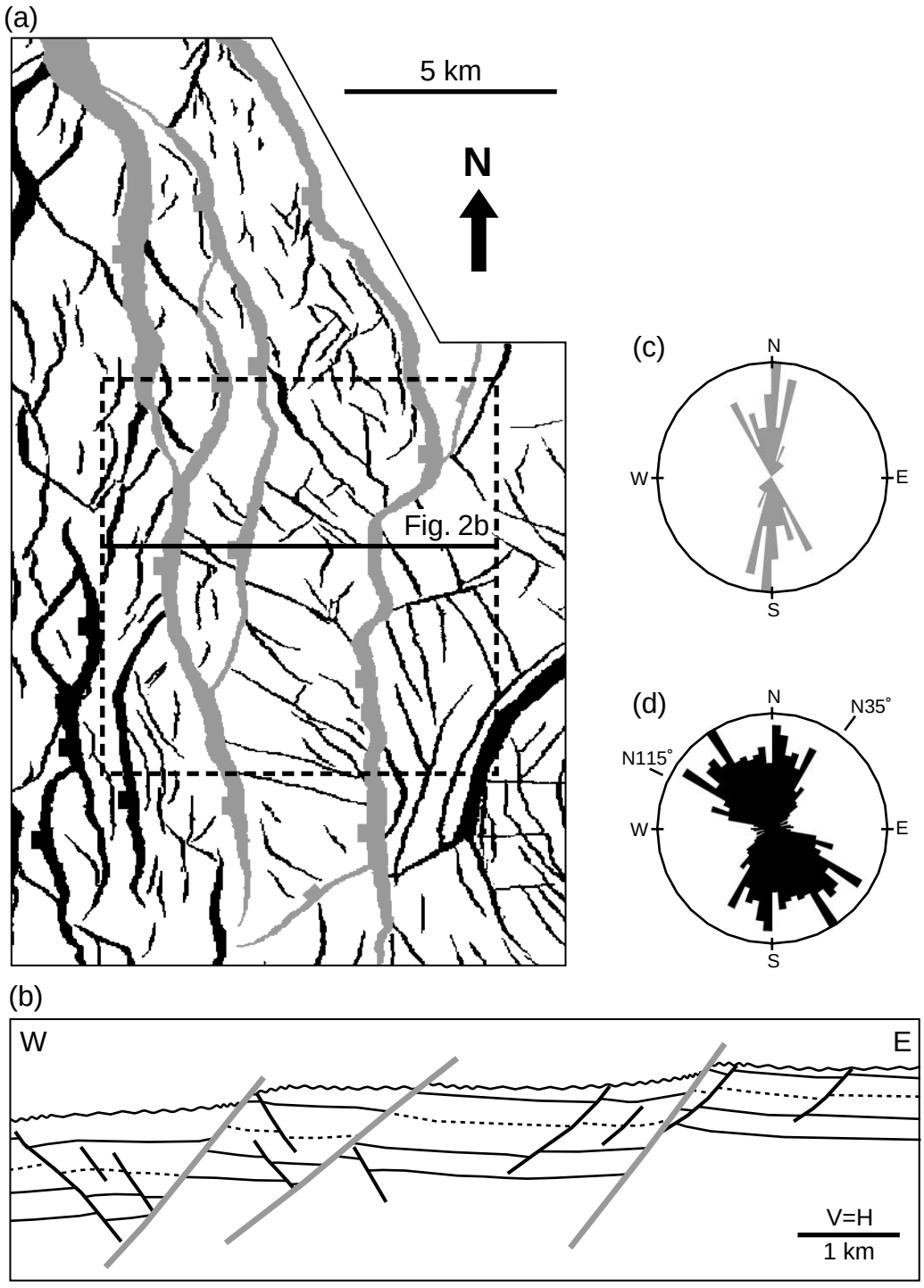

Fig. 2. The Oseberg Syd area. (a) Fault map of the Base Brent horizon. Gray faults are the major west-dipping, ~N–S striking normal faults (Lower to Upper Jurassic age). Black smaller faults have much more variable orientation and are later, being predominantly Upper Jurassic. The dashed box delineates the Oseberg Syd subregion selected for detailed study (see Figs.4 and 5). (b) Cross-section across the studied area (see (a) for location). Dashed line is the faulted horizon of (a). This seismic horizon is used to position the observation points (see Fig. 4). (c) Azimuth frequency diagram of the major ~N–S striking normal faults. (d) Azimuth frequency diagram of the smaller Upper Jurassic normal faults. N115 to N35° represents the range of smaller fault orientations.

several deformation phases, each with a particular extension or contraction direction and magnitude, can be represented as remote stress or strain boundary conditions.

Based on this, one can compute the perturbed stress/strain fields at observation points (see Fig. 3) in the surrounding rock volume as a result of the observed subsurface fault plane geometries, associated slip distribution, and remote strain or stress field.

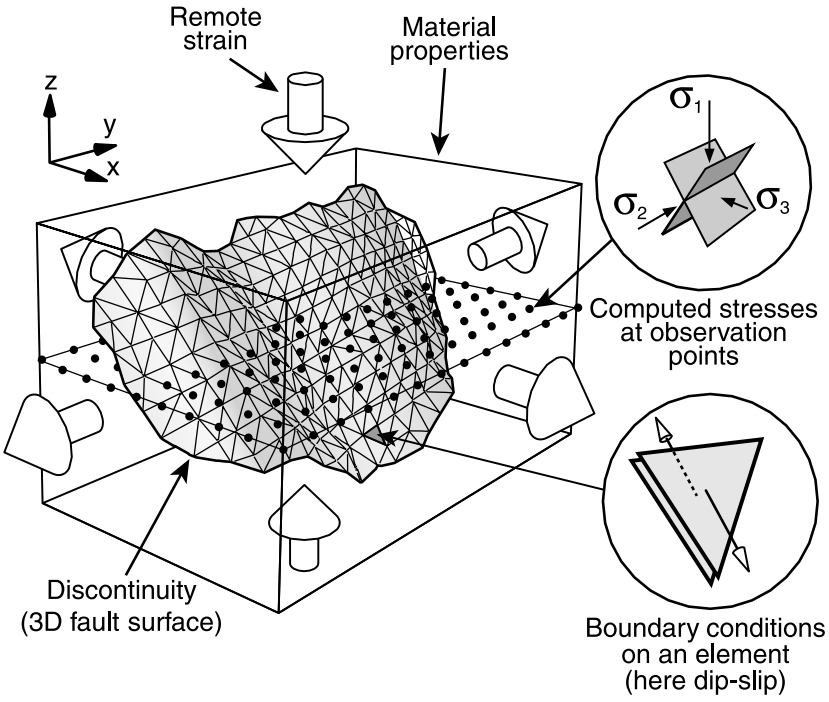

Fig. 3. Schematic representation of a Poly3D model configuration. The discretization of 3D fault surface into triangular boundary elements allows the construction of a surface of any desired tipline shape. Boundary conditions can be applied remotely and locally, at the center of each element discontinuity. Output at observation points (black dots) can be magnitude and orientation of principal stresses.

3.1. Model configuration

The models were constrained with appropriate local and remote boundary conditions. The large, early faults (Fig. 4) were directly incorporated into the mechanical models. Displacement discontinuity on all faults was constrained to be pure dip-slip and the amount of dip-slip, used as the local boundary condition for each element, was determined directly from 3D seismic data interpretation and fault analysis.

The 3D strain, estimated from palinspastic restoration (Rouby et al., 1993) of the seismic horizons over the entire area (Maerten, 1999), was used as the remote boundary condition:

$\varepsilon_{N80^\circ} = 0.13$ (~E–W strain)

$\varepsilon_{N170^\circ} = 0.04$ (~N–S strain)

$\varepsilon_V = -0.17$ (~vertical strain)

where ε_i represents one of the three principal strains.

Two elastic constants, Poisson's ratio and Young's modulus, were used to characterize the behavior of the linear elastic and isotropic solid. We used a value of 0.15 for Poisson's ratio and 65 GPa for Young's modulus, which are typical values for loose sand (Clark, 1966). We believe that these values adequately represent the reservoir lithology at the time of deformation.

3.2. Model output

The stress tensor was calculated at observation points in the volume around the faults. The observation points were placed, with a 200 m horizontal spacing, on a $9 \times 9\ km^2$ square grid on the Base Brent horizon (Figs. 2 and 4). The computed principal stress axes were combined with a failure criterion to determine both the expected fault density and the expected fault strike.

We used the maximum Coulomb shear stress (Jaeger and Cook, 1979, p. 95) as an index for fault density. This criterion has been used by Crider and Pollard (1998) to interpret secondary faulting at a breached relay between overlapping normal faults (Childs et al., 1995). The value of the maximum Coulomb shear stress is determined by:

$$S_c = \left(\frac{(\sigma_1 - \sigma_3)}{2}\sqrt{1+\mu^2}\right) - \mu\left(\frac{(\sigma_1 + \sigma_3)}{2}\right)$$

where σ_1 and σ_3 are the maximum and minimum principal stresses and μ is the coefficient of internal friction, taken to be 0.6.

The fault orientations were estimated using the Coulomb failure criterion (Jaeger and Cook, 1979, p. 95) defined by:

$$\tan 2\theta = -\frac{1}{\mu}$$

where θ is the angle of the failure planes to the maximum principal compressive stress (σ_1) and μ is the coefficient of internal friction. Two conjugate failure planes intersect

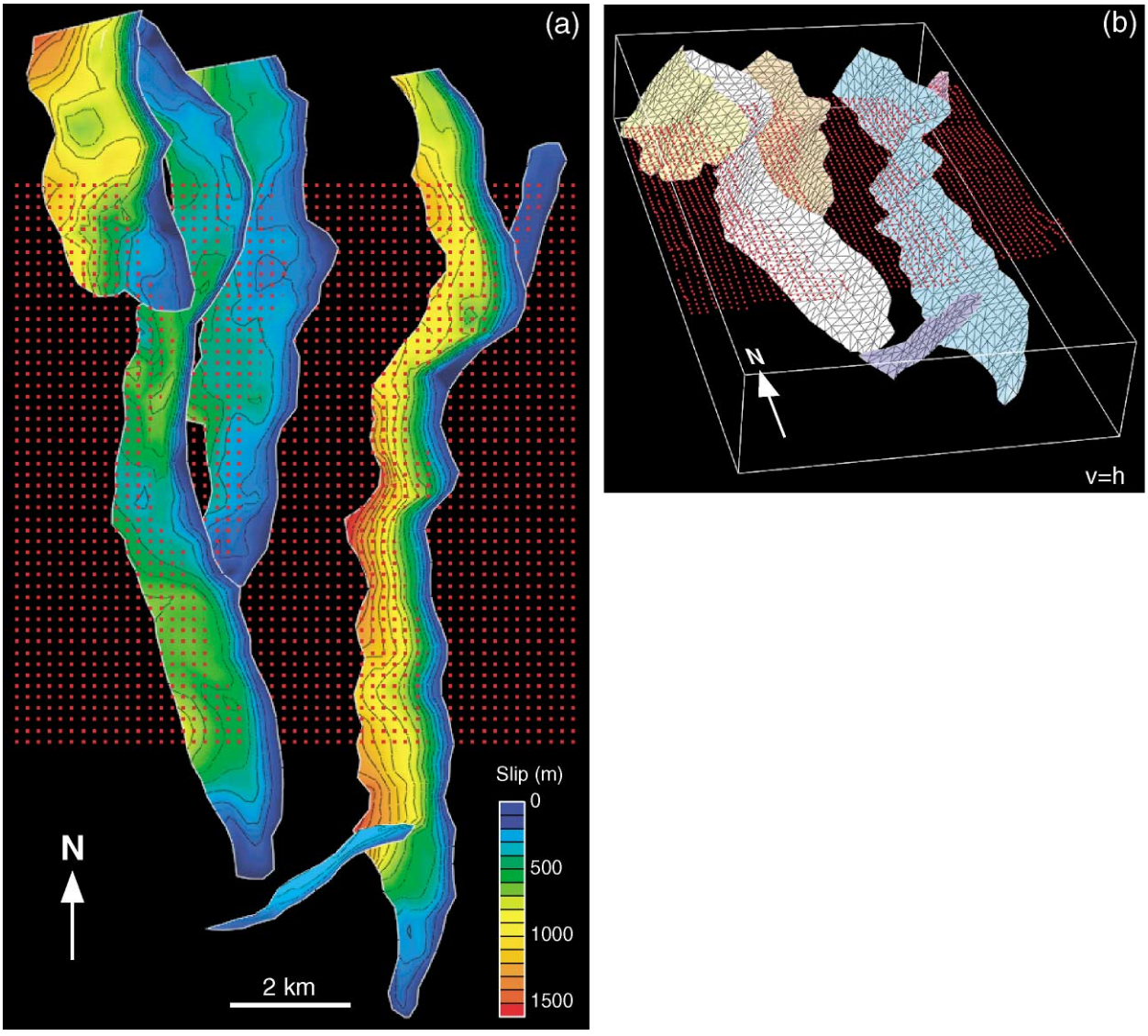

Fig. 4. Model configuration. (a) Interpreted dip-slip distribution used as local boundary condition. Contour interval of slip is 100 m. (b) A 3D view of the model mesh made of triangular elements. Red dots are observation points located on a seismic horizon going through the faults.

along σ_2 (Fig. 3) and the fault orientation is influenced only by the orientation of the principal stresses.

4. Model results

4.1. Fault density

The magnitude of S_c is represented as a color-coded map in Fig. 5a. For comparison, a fault density map has been generated (Fig. 5b) by summing the product of the length and the displacement of all the fault segments inside a $1000 \times 1000\ m^2$ window, panned across the area with a step of 200 m in both the E–W and N–S directions. This measure of density is similar to the geometric moment (e.g. Westaway, 1994) and is related to the strain caused by faulting. To facilitate comparison, the values for the observed and the computed data have been normalized into uniform distributions with values ranging from zero to one.

The highest observed and predicted densities occur at bends, which act as stress concentrators. Highest densities are also found close to faults that present the highest dip-slip values (see Fig. 4a), as seen along the eastern most ~N–S fault of the model. Further away from the largest faults there are lower predicted densities that result from the stress relief caused by faulting.

Correlations between predicted and measured densities are best in the central region of the model. Large faults outside the model volume may have perturbed the intensity of secondary faults near the edges of the model, leading to poorer correlation.

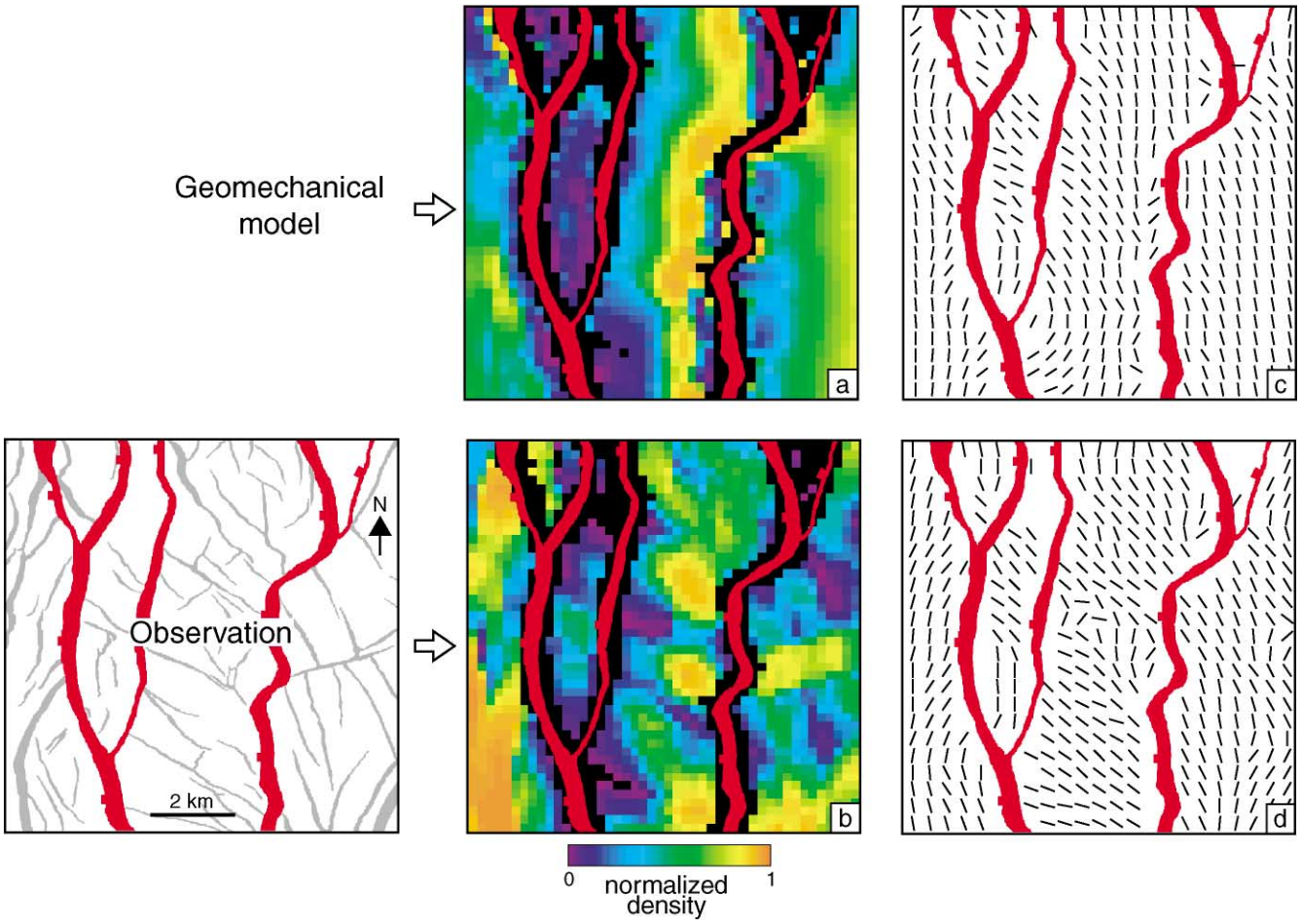

Fig. 5. Comparison between computed and observed fault density and fault strike. (a) Computed fault density using the major ~N–S (red) faults in the mechanical model and a remote loading with a N80° direction of extension. (b) Density of the observed Upper Jurassic (gray) faults. All densities reported as normalized values from zero to one. See text for details. (c) Computed fault strike for the same model as (a). (d) Average strike of the observed gray faults.

4.2. Fault strike

As σ_1 is everywhere nearly vertical in the model results, the strike of the two Coulomb failure planes is approximately given by the direction of σ_2 and so this direction was used to estimate fault strike. The strike map of the interpreted smaller faults was generated using a similar method to that previously described for the observed density (Fig. 5d). The average strikes were calculated within the scan window by vector summation of the fault segments, the norm of the vectors being weighted by the product of length and displacement of each segment (e.g. Maerten, 1999).

The strike map derived from numerical modeling is shown in Fig. 5c. Far away from the faults, the stress system is similar to the applied remote stress, with the maximum compression vertical and the predicted faults being normal faults, striking N170°. However, results show a close correlation between the computed strikes over most of the area and the observed strikes of the smaller faults. Local variations in strike close to large faults are well represented. Secondary faults curve close to bends along the major faults and close to fault intersections where the stress perturbations are the greatest. A nice example of close correlation is within the third faulted block from the west, where secondary faults curve close to major fault intersections. Some misfits occur in several regions of the model. For example in the south-central region where the predicted fault strike is wrong by up to 90°. The misfit could be explained by large faults outside of the modeled area that have not been included in the model. These faults may as well be deeper basement faults.

4.3. Extension direction

A series of models were run in order to quantitatively investigate the effect of the remote extension direction on the predicted strike of the smaller faults. The direction of the principal extension was varied from N50 to N120° with steps of 10° by modifying the principal remote strains accordingly. The results, shown in Fig. 6, represent the discrepancy angle, ranging from 0 to 90°, between the observed and computed strikes, computed at each observation point. The first column of Fig. 6 is the histogram

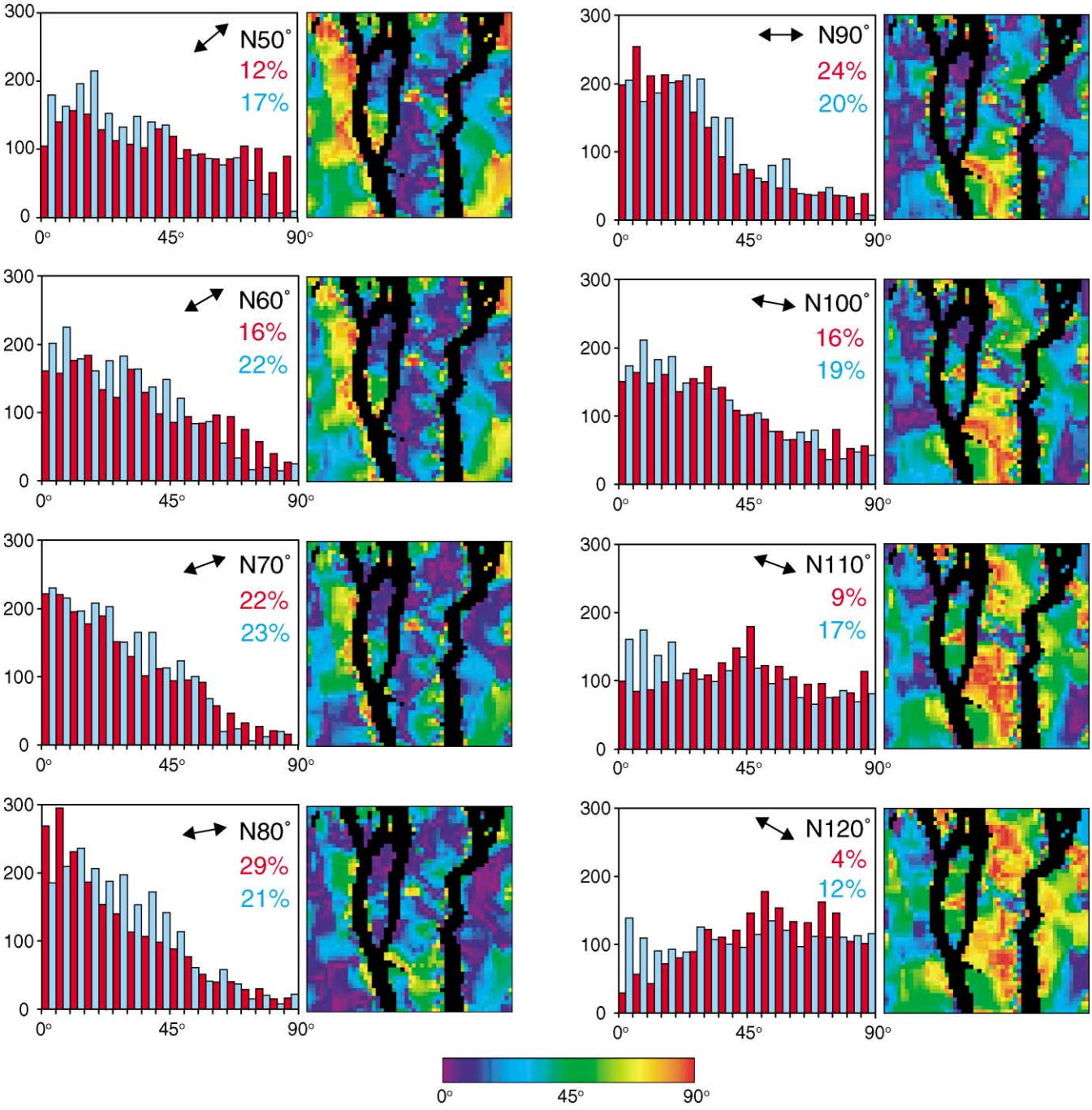

Fig. 6. Discrepancy angle between the observed and computed strike plotted on a histogram (red bars on the left column) and on a color-coded map (right column) for eight separate models with a direction of extension varying from N50 to N120° with a step of 10°. Histograms with blue bars represent the discrepancy angle between the observed strikes and the computed strikes for a homogeneous stress field. Numbers in histograms are the percentage of data that fall between 0 and 10° discrepancy.

(red bars) of the discrepancy angle and the second column represents the color-coded map of the same angle. As a control, histograms are also given (blue bars) of the discrepancy angle between the observed strikes and the computed strikes assuming that the large scale faults had no influence on the stress orientations. These control histograms (blue bars) correspond to models with a homogeneous stress field, whereas the red bar histograms correspond to models with a heterogeneous stress field perturbed by major fault slip.

Model results (Fig. 6) show that a N80° direction of extension gives the best fit between computed — with homogeneous and heterogeneous stress fields — and observed strikes: 29% of the data have a discrepancy angle less than 10° (red bars), compared with 21% for the control case (blue bars). Most of the other models give a

better fit with a homogeneous stress field; however, the percentage of the data that have a discrepancy angle less than 10° are always much lower than the 29% of the best model (e.g. N80°). The general shape of the histograms is also an indicator of the goodness of fit — flat histogram means that the fit is poor (e.g. N50 or N110°), whereas rapid decay with increasing discrepancy angle (e.g. N80 or N90°) means that the model is, in general, better. This analysis suggests that the large-scale faults had an impact on the orientation of the smaller faults. The color-coded maps of Fig. 6 support this conclusion, showing that a N80° direction of extension produces the most uniform distribution of small discrepancy angles (cool colors). In contrast, the other directions of extension produce larger zones where the discrepancy is high (warm colors). The misfits of the fault strike described earlier, especially in the central southern region, are also underlined with the color-coded map of the discrepancy angle (see Fig. 6, N80° case).

5. Discussion and conclusions

The present study leads to a possible physical explanation for the observed secondary fault strike variations and clusters in the Oseberg area. We have shown that, despite the limitations of our modeling technique (in terms of inelastic deformation, spatial variation of material properties and fault growth discussed in Maerten et al. (1999)), elastic deformation around faults produces stress perturbations consistent with the orientations and densities of smaller secondary faults in the natural data set. These correlations suggest that an elastic deformation model, when populated with realistic fault geometries and boundary conditions, captures the first order variations in the stress field. Apparently, the strike variations of secondary faults can be the result of stress perturbations around larger faults, and need not be explained by invoking multiple tectonic episodes or control by basement lineaments.

Our results indicate that a N80° extension direction produces a better correlation between computed and observed fault strikes than the regional Upper Jurassic NW–SE direction of extension (e.g. N120°, Fig. 6) proposed by Færseth et al. (1997). This suggests two hypotheses, consistent with the model results presented here, regarding the Jurassic northern North Sea direction of extension. The first is that the NW–SE regional extension is perturbed locally to become N80° in the Oseberg area. For example, the rift is bounded by large crustal faults that are oblique to the overall graben trend (Færseth et al., 1997). This obliquity of the major faults could cause a local reorientation of the stress field. The second hypothesis is that the E–W direction of extension (Roberts et al., 1990; Brun and Tron, 1993) was stable throughout the Jurassic time. Future investigations will test these hypotheses.

The conclusions of this study are dependent upon the timing of the faulting. Although in the example used here the smaller faults did generally form during the last stage of development of the larger faults, and therefore could be influenced mechanically by them; this is not necessarily true in all sequences. Indeed, it is to be expected in a population of growing faults that small faults would develop early and stop growing before their orientation and density are affected by the stress perturbation around later larger faults. In addition, the geometry of the larger faults themselves may have evolved with time, such that secondary faulting occurred under somewhat different stress states than those modeled here.

We have only considered the scale of faulting represented by the seismic data set. This includes faults ranging from 0.5 to 15 km in the horizontal dimension with displacements ranging from 30 to 700 m. We have demonstrated that the smaller faults may have been influenced by the larger faults within this seismic data set. It is likely that this process occurs over the full range of fault scales. Thus, faults at the subseismic scale (maximum displacement <30 m) would have orientations and densities related to the stress perturbations of the seismic-scale faults.

The techniques presented here highlight important implications for the prediction of subsesimic faults in reservoirs or aquifers. By bringing all of the faults that are resolvable in the sesimic data into the mechanical model, it may be possible to predict the orientations and densities of subseismic faults. Such subseismic fault models could be used in reservoir modeling or well-planning. This is a topic that will be considered elsewhere.

Acknowledgements

This research was supported by Norsk Hydro Research Center (Norway) and the Stanford Rock Fracture Project. Special thanks to Wenbing Zhang and Frantz Maerten for their computer skills and help. Thanks also to Chris Dart, Nils Telnas and Ridvan Karpuz for encouragement and to Patience Cowie and Bill Shea for reviewing the manuscript.

References

Ackermann, R.V., Schlische, R.W., 1997. Anticlustering of small normal faults around larger faults. Geology 25, 1127–1130.

Becker, A.A., 1992. The Boundary Element Method in Engineering. McGraw-Hill, New York.

Brun, J.-P., Tron, V., 1993. Development of the North Viking Graben: inferences from laboratory modelling. Sedimentary Geology 86, 31–51.

Childs, C., Watterson, J., Walsh, J.J., 1995. Fault overlap zones within developing normal fault systems. Journal of Geological Society, London 152, 535–549.

Clark Jr, S.P. (Ed.), 1966. Handbook of Physical Constants (revised edition). Geological Society of America Memoir 97.

Couples, G., 1977. Stress and shear fracture (fault) patterns resulting from a suite of complicated boundary conditions with applications to the Wind River Mountains. Pure and Applied Geophysics 115, 113–133.

Cowie, P.A., 1998. A healing-reloading feedback control on the growth rate of seismogenic faults. Journal of Structural Geology 20, 1075–1087.

Crider, J.G., Pollard, D.D., 1998. Fault linkage: 3D mechanical interaction between overlapping normal faults. Journal of Geophysical Research 103, 24,373–24,391.

Crouch, S.L., Starfield, A.M., 1983. Boundary Element Methods in Solid Mechanics: with Applications in Rock Mechanics and Geological Engineering. Allen & Unwin, Winchester, MA.

Færseth, R.B., Knudsen, B.-E., Liljedahl, T., Midbøe, P.S., Søderstrøm, B., 1997. Oblique rifting and sequential faulting in the Jurassic development of the North Sea. Journal of Structural Geology 19, 1285–1302.

Færseth, R.B., Ravnås, R., 1998. Evolution of the Oseberg Fault-Block in context of the northern North Sea structural framework. Marine and Petroleum Geology 15, 467–490.

Fristad, T., Groth, A., Yielding, G., Freeman, B., 1997. Quantitative fault seal prediction — a case study from Oseberg Syd. In: Moller-Pedersen, P., Koestler, A.G. (Eds.), Hydrocarbon Seals, Importance for Exploration and Production. Norwegian Petroleum Society (NPF) Special Publication 7, pp. 107–124.

Gupta, S., Cowie, P.A., Dawers, N.H., Underhill, J.R., 1998. A mechanism to explain rift-basin subsidence and stratigraphic patterns through fault-array evolution. Geology 26, 595–598.

Hafner, W., 1951. Stress distribution and faulting. Bulletin of the Geological Society of America 62, 373–398.

Jaeger, J.C., Cook, N.G.W., 1979. Fundamentals of Rock Mechanics. Chapman and Hall, London.

Kattenhorn, S.A., Aydin, A., Pollard, D.D., 2000. Joints at high angles to normal fault strike: an explanation using 3-D numerical models of fault-perturbed stress fields. Journal of Structural Geology 22, 1–23.

Krantz, R.W., 1989. Orthorhombic fault patterns: the odd axis model and slip vector orientations. Tectonics 8, 483–495.

Maerten, L., 1999. Mechanical interaction of intersecting normal faults: theory, field examples and applications. Ph.D. thesis, Stanford University, California.

Maerten, L., Willemse, M.J., Pollard, D.D., Rawnsley, K., 1999. Slip distributions on intersecting normal faults. Journal of Structural Geology 21, 259–271.

Maerten, L., Pollard, D.D., Karpuz, R., 2000. How to constrain 3-D fault continuity and linkage using reflection seismic data: a geomechanical approach. American Association of Petroleum Geologists Bulletin 84, 1311–1324.

Maerten, L., 2000. Variation in slip on intersecting normal faults: implications for paleostress inversion. Journal of Geophysical Research 105, 25,553–25,565.

Pollard, D.D., Segall, P., 1987. Theoretical displacements and stresses near fractures in rock: with application to faults, joints, veins, dikes, and solution surfaces. In: Atkinson, B.K. (Ed.), Fracture Mechanics of Rock. Academic Press, London, pp. 277–349.

Reches, Z., 1983. Faulting of rocks in three-dimensional strain fields, II: theoretical analysis. Tectonophysics 95, 133–156.

Roberts, A.M., Yielding, G., Badley, M.E., 1990. A kinematic model for the orthogonal opening of the Late Jurassic North Sea rift system, Denmark, Mid Norway. In: Blundel, D.J., Gibbs, A.D. (Eds.), Tectonic evolution of the North Sea rifts. Clarendon Press, Oxford, pp. 180–199.

Rouby, D., Cobbold, P.R., Szatmari, P., Demerican, S., Coelho, D., Rici, J.A., 1993. Least-squares palinspastic restoration of region of normal faulting-application to the Campos basin (Brasil). Tectonophysics 221, 439–452.

Sassi, W., Faure, J.-L., 1997. Role of faults and layer interfaces on the spatial variation of stress regimes in basins: inferences from numerical modelling. Tectonophysics 266, 101–119.

Schlische, R.W., Young, S.S., Ackermann, R.V., Gupta, A., 1996. Geometry and scaling relations of a population of very small rift-related normal faults. Geology 24, 683–686.

Thomas, A.L., 1993. Poly3D: a three-dimensional, polygonal-element, displacement discontinuity boundary element computer program with applications to fractures, faults, and cavities in the Earth's crust. M.S. thesis, Stanford University, California.

Westaway, R., 1994. Quantitative analysis of populations of small faults. Journal of Structural Geology 16, 1259–1273.

Willemse, J.M., 1997. Segmented normal faults: correspondence between three-dimensional mechanical models and field data. Journal of Geophysical Research 102, 675–692.

Willemse, J.M., Pollard, D.D., Aydin, A., 1996. Three-dimensional analyses of slip distribution on normal fault arrays with consequences for fault scaling. Journal of Structural Geology 18, 295–309.

Yielding, G., Badley, M.E., Roberts, A.M., 1992. The structural evolution of the Brent Province. In: Morton, A.C., Haszeldine, R.S., Giles, M.R., Brown, S. (Eds.), Geology of the Brent Group. Special Publication of the Geological Society of London 61, pp. 27–40.